Multiphysics Finite-Element Modeling of the Neuron/Electrode Electrodiffusive Interaction

Federico Leva[1*†], Claudio Verardo[2,3†], Leandro Julian Mele[2], Pierpaolo Palestri[2], Luca Selmi[1]
[1]*Department of Engineering "Enzo Ferrari", University of Modena and Reggio Emilia, Modena, Italy*
[2]*Polytechnic Department of Engineering and Architecture, University of Udine, Udine, Italy*
[3]Now with: *Maastricht Centre for Systems Biology, Maastricht University, Maastricht, The Netherlands*
[*]E-mail: federico.leva@unimore.it

***Abstract*—Understanding the biological-electrical transduction mechanisms is essential for reliable neural signal recording and feature extraction. As an alternative to state-of-the-art lumped-element circuit models, here we adopt a multiscale-multiphysics finite-element modeling framework. The model couples ion transport with the Hodgkin-Huxley model and the readout circuit, and is used to investigate a few relevant case studies. This approach is amenable to explore ion transport in the extracellular medium otherwise invisible to circuit model analysis.**

***Index Terms*—neural recording, extracellular sensing, FEM, neural signal transduction, Hodgkin-Huxley**

I. Introduction

The interaction of complementary metal-oxide-semiconductor (CMOS) electronics with biological entities [1], [2] represents today a challenging multiphysics and multiscale case study in the field of neuroscience, given the different nature, scales, and physical properties of the system components. Multiscale-multiphysics finite-element modeling (FEM) and simulation platforms [3], [4] perfectly serve the aim of estimating the neuron/electrode interaction in well defined physical conditions. They allow to gain insight on the transduction processes and derive more accurate and physics-based lumped-element circuit models [5]–[8].

In previous works [9], [10], we developed a simulation methodology to study sensing devices coupled to neurons using a mixed-mode device-circuit simulator for semiconductor devices [3]. Here we extend and improve our approach and embrace a general purpose multiphysics FEM platform [4] that naturally includes distributed time-dependent transport of ionic and electronic carriers.

II. Methodology and Validation

In our work we used [4] which enables the physical description of the domains of interest: the intra- and extracelluar electrolytes, the neuron membrane, the metallic/semiconductor electrode and the related readout circuitry, as showcased in Fig. 1 where the model equations are also defined.

An electrolyte region is described via its relative permittivity, and the number, valence, and diffusivity of the soluted ion species. It is described with the *Poisson-Nernst-Plank* (PNP) transport model [13] (Eqs. 1-3), implemented via a multiphysical coupling between the *electrostatics* and *transport of diluted species* interfaces from the AC/DC and electrochemistry modules [4], respectively. A *reference electrode* (RE in Fig. 1) is inserted in the simulation to set the ground potential reference in the bulk of the extracellular fluid.

The neuron membrane is treated as an insulator using a thin layer approximation instead of a fine mesh, enforcing the continuity of the normal component of the displacement field vector across the intra- and extracellular boundaries (Eq. 8) so that electrical double layers (EDLs) build up at these interfaces. The dynamics of the ionic channels embedded at each grid point of the membrane are described via the Hodgkin-Huxley (HH) formalism [12], [14] assuming rest membrane potential V_r=-65 mV. The HH's gating variables are computed solving a set of ordinary differential equations (ODE) at each membrane mesh point (Eq. 6); consequently, the corresponding currents of the ionic channels are updated as in Eq. 7, and applied as boundary fluxes to the electrolyte fluids according to Eq. 9. The transmembrane stimulus to elicit action potentials (APs) is applied as additional Na^+ boundary flux as simplified model of excitatory synapses [15]. The membrane potential, V in Eq. 4, is the voltage controlling the non-linear conductances, whereas the reversal potentials for the ions are either: i) directly included as constant parameters in the ODEs (see caption of Fig. 1); or ii) updated by sampling the ionic concentration at each time-step assuming that changes in the concentrations instantaneously turn into changes in potential through Eq. 5. The sampling is performed at 6 nm from the cell membrane (i.e., more than than five times the Debye length of the electrolyte [13]) to ensure an almost complete decay of the EDL. Option (ii) entails that we self-consistently account for the impact of extracellular concentrations on the membrane potential. To the best of our knowledge, this is a unique and novel feature of our approach for the modeling of the neuron/electrode interface.

The sensing electrode is modeled as a metal with finite conductivity and permittivity (Eq. 12) through the *electric current* interface of the AC/DC module [4]. Assuming no *redox* reactions at its interface, we include a Stern layer via the thin layer approximation also used for the membrane, which leads to the formation of a diffuse layer in the electrolyte (Eq. 10). The displacement current entering the electrode from

[†]These authors contributed equally to the work. This work has been financially supported by the European Union's Horizon-2020 project "IN-FET" (Grant Agreement n. 862882) vie the IUNET consortium.

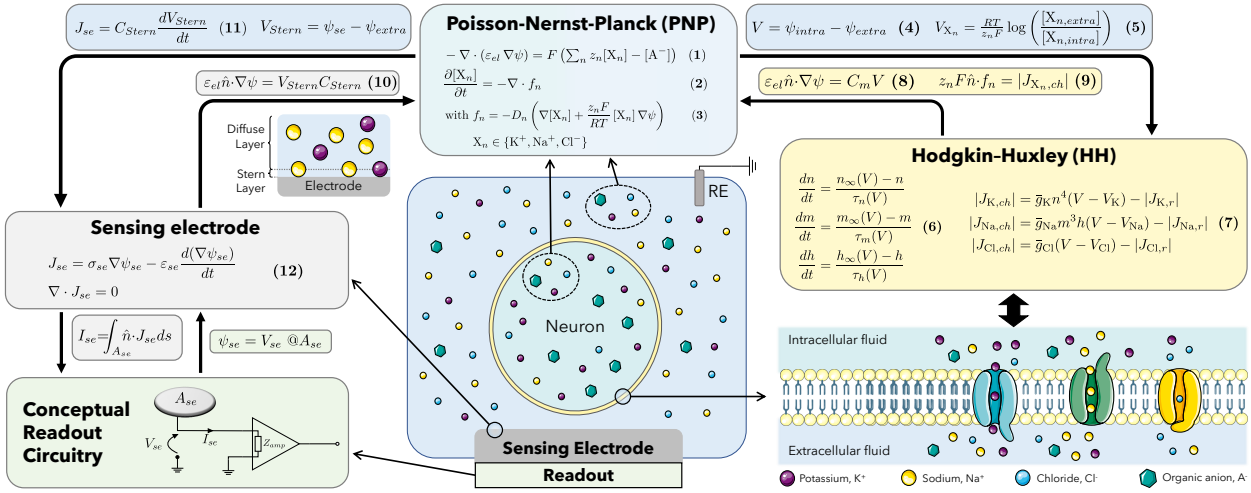

Physical variables: ψ=electrolyte electric potential, $[\mathrm{X}_n]$=concentration of a mobile ion, $[\mathrm{A}^-]$=concentration of fixed anions, f_n=ion flux, n, m, h=gating variables, J_{X_n}=ion channel current density, $J_{\mathrm{X}_{n,r}}$= J_{X_n} evaluated at rest potential, V_{X_n}=reversal potential, V=membrane potential, V_{Stern}=Stern layer potential, J_{se}=electrode electric current density, ψ_{se}=electrode electric potential, I_{se}=readout input current, V_{se}=readout input voltage. **Physical parameters:** ε_{el}=electrolyte electric permittivity, D_n=ionic diffusivity, z_n=ionic valence, $n_\infty, m_\infty, h_\infty$=(in)activation curves of gating variables, τ_n, τ_m, τ_h=time constants of gating variables, $\bar{g}_{\mathrm{X}_n}$=maximum ion channel conductance, C_m=membrane capacitance, C_{Stern}=Stern layer capacitance, σ_{se}=electrode conductivity, ε_{se}=electrode permittivity, T=temperature, F=Faraday constant, R=gas constant, A_{se}=electrode surface area, Z_{amp}=readout input impedance. (Image adapted from Servier Medical Art, © CC BY 3.0)

Fig. 1: Sketch of the modeling framework: neuron membrane, cellular fluids, sensing electrode, and readout circuitry. The boxes represent different physics, mutually coupled by the equations on the connecting arrows. If not otherwise specified the parameters of the PNP and electrode models (e.g., gold electrode conductivity) are taken from [11]. Those of the HH model are taken from [12]. The ion concentrations at the reference electrode (RE) are set to typical extracellular values: $[K^+]$=5 mM, $[Na^+]$=130 mM, $[Cl^-]$=135 mM, while in the intracellular fluid they are computed to match the baseline reversal potentials V_K=-77 mV, V_{Na}=50 mV, V_{Cl}=-54.4 mV. The fixed charges A^- are set to yield electroneutrality. C_{Stern}=55.6 μF/cm^2. T=23° C.

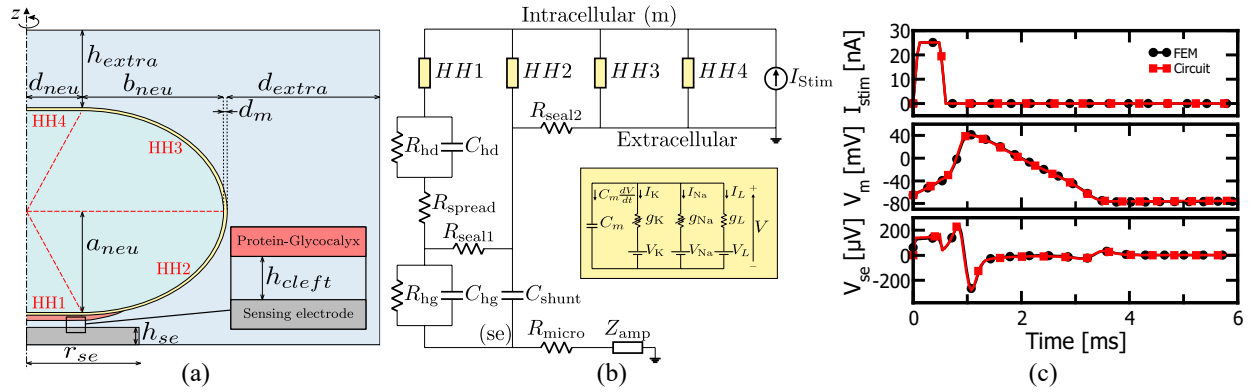

Fig. 2: Comparison between the proposed simulation deck that naturally embodies a distributed description of the system and an equivalent lumped-element circuit approach: (a) 2D cross-section (not to scale) of the 3D FEM domain with cylindrical symmetry around the z-axis, modeling an ellipsoidal neuron in proximity of a planar sensing electrode that is connected to the same Z_{amp} of panel b. Default parameters are: h_{extra}=d_{extra}=a_{neu}=40 μm, d_{neu}=r_{se}=10 μm, b_{neu}=67 μm, d_m=10 nm, h_{cleft}=90 nm, h_{se}=0.2 μm. (b) Lumped-element circuit model derived from [11] splitting the neuron into four compartments (yellow boxes). Default values are: R_{hd}=510 MΩ, C_{hd}=2.2 pF, R_{spread}=7.7 MΩ, R_{seal1}=600 kΩ, R_{seal2}=8 kΩ, R_{hg}=140 kΩ, R_{micro}=14 μΩ, C_{hg}=106 pF, C_{shunt}=4 pF, Z_{amp}=R_{amp}=100 GΩ. (c) Waveforms of imposed transmembrane stimulus current (top panel), resulting APs (middle panel) and sensed signal (bottom panel) from the models a and b, respectively.

the Stern layer originates from the *normal current density* boundary condition (Eq. 11). The electrode is connected to the input impedance of an ideal amplifier although our approach can include readout circuits of any complexity.

To validate the proposed methodology we define a FEM domain with physical properties and dimensions taken from a reference model [11] that implements a lumped-element circuit description of the neuron/electrode interaction and action potential generation capability via HH circuits [16]. The model accuracy in [11] is validated against literature data.

Fig. 2.a sketches a 2D cross-section of the 3D FEM domain with cylindrical symmetry around the z-axis, representing an ellipsoidal neuron in proximity of a planar electrode. We account for the protein-glycocalyx layer at the bottom of the neuron [5], [6], [11] by setting the ion diffusivities in this domain so as to reproduce the resistivity reported

in [11]. Fig. 2.b illustrates the lumped-element equivalent circuit obtained, as in [11], by partitioning the neuron into four HH compartments, each with parameters proportional to the respective membrane surface area. We neglect the series resistances between adjacent HH compartments given that the intracellular compartment behaves like an equipotential space due to its large dimensions. All lumped-elements in the circuit have been computed as in [11] except for R_{seal1} and R_{seal2} that are adjusted so that the circuit's waveforms match the FEM's ones, and Z_{amp} which accounts for the presence of a readout circuitry. Fig. 2.c compares the AP waveform elicited by a transmembrane stimulating current (top panel) applied to the compartment HH4 in Fig. 2.a and b. The resulting intracellular (middle panel) and sensed (bottom panel) waveforms show full agreement between our FEM model and [11] demonstrating the credibility of the approach w.r.t. state-of-the-art results.

III. Results and Conclusions

We now analyze a few relevant case studies with the new modeling framework. Fig. 3 collects the signal sensed by the electrode during transient responses to action potentials (a) for variations of one parameter at a time and constant reversal potentials (b-d), and for default parameter values and sampled reversal potentials (e). During each study, the other parameters are kept at their default value (see caption of Fig. 2).

All the APs are elicited by means of the same transmembrane current stimulus (Fig. 2.c, top panel) applied to the region HH4 of Fig. 2.b, thus yielding the same intracellular potential profiles (Fig. 3.a). However, when the current stimulus reaches the extracellular fluid it causes an artifact in the recorded signal waveforms (i.e., the peak between 0-0.5 ms in Fig.3 b-e). After that, the extracellular dynamics and the resulting waveforms (i.e., profiles, and peaks amplitude and location in Fig.3 b-e) remain unaffected by the artificial stimulus but only depend on the electrogenesis and electrodiffusion.

Fig. 3 shows the principal trends: b) the lower the cleft thickness, the larger the amplitude of the recorded signal as the neuron/electrode sealing increases (as in [11]); c) a too small electrode entails weak coupling and sealing with the neuron whereas a too large electrode entails strong coupling with the grounded extracellular environment rather than with the neuron, implying an optimal size of ≈10 µm in our study; d) the larger the amplifier's input impedance (i.e., large R_{amp} or small C_{amp}), the larger the sensed signal as the readout strongly dominates the potential divider with the electrode (and possibly the interconnects). In the aforementioned studies the reversal potentials of the neuronal membrane are kept fixed for the sake of a qualitative comparison with the circuit-level modeling studies from literature.

Fig. 3.e shows the sensed signals induced by two consecutive APs elicited 30 ms apart from each other. Differently from the previous analyses, now the membrane reversal potentials change consistently to the ion concentrations (Eq. 5), that in general are time-dependent. In particular, V_K drifts from -77 mV to -36.5 mV (not shown) due to the accumulation of K^+ ions emitted in the protein-glycocalyx layer during the first

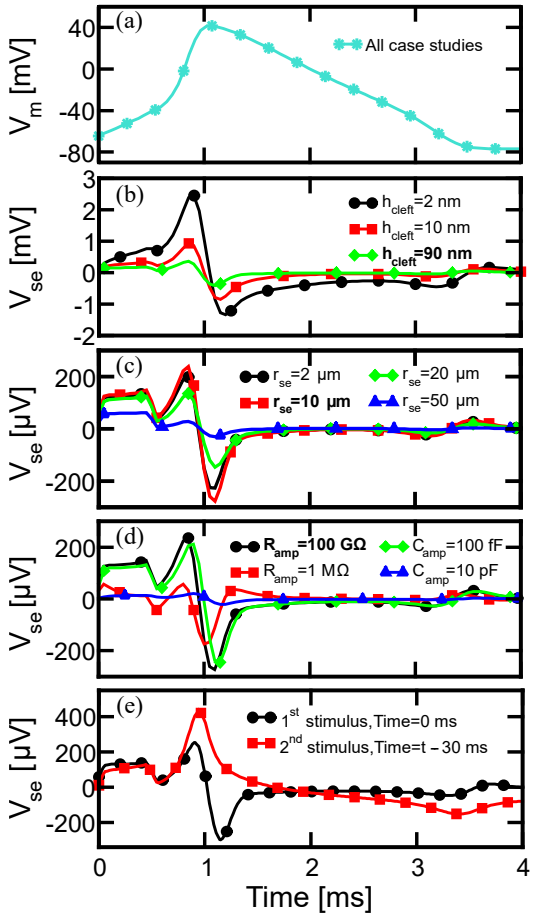

Fig. 3: (a) Elicited action potential (AP) waveform; (b-e) corresponding signals sensed by the electrode for constant (b-d) and sampled (e) reversal potentials. The parameters swept from the default values (in bold) for parametric studies are: cleft thickness (b), radius of the sensing electrode (c), amplifier's input impedance (either a resistance R_{amp} or a capacitance C_{amp}) (d); the same signals are recorded for repeated APs (not shown). The analysis with sampled reversal potentials (e) has default parameters (see caption of Fig. 2) but depends on the previous stimulation pulses. The V_{se} waveforms obtained by two consecutive pulses (at 0 and 30 ms) are shown superimposed for comparison.

AP, whose diffusivity is approximately 10^6 smaller than in the extracellular fluid. Such a low diffusivity is consistent with the high resistivity provided in [11], but the observed impact on the V_{se} waveform highlights the importance of self-consistent models and asks for further in-depth investigations to improve the FEM model of the protein-glycocalyx layer, combining its electrodiffusive effects with a more realistic ionic homeostasis.

In conclusion, the proposed simulation framework accurately reproduces the results of state-of-the-art circuit models of the neuron/electrode interaction. It also enables the investigation of fundamental hypotheses regarding macroscopic aspects of the model (e.g., the protein-glycocalyx layer impedance). Finally, it helps shed light on the ion transport phenomena that ultimately affects the transduced signals.

REFERENCES

[1] G. Zeck, F. Jetter, L. Channappa, G. Bertotti, and R. Thewes, "Electrical imaging: investigating cellular function at high resolution," *Advanced Biosystems*, vol. 1, no. 11, p. 1700107, 2017. 10.1002/adbi.201700107.

[2] J. Abbott, T. Ye, K. Krenek, R. S. Gertner, W. Wu, H. S. Jung, D. Ham, and H. Park, "Extracellular recording of direct synaptic signals with a cmos-nanoelectrode array," *Lab Chip*, vol. 20, pp. 3239–3248, 2020. 10.1039/D0LC00553C,.

[3] Synopsys, Inc., Sentaurus Device v. N-2017.09.

[4] Comsol, Inc., Comsol Multiphysics v. 6.0.

[5] V. Thakore, P. Molnar, and J. J. Hickman, "An optimization-based study of equivalent circuit models for representing recordings at the neuron–electrode interface," *IEEE Transactions on Biomedical Engineering*, vol. 59, no. 8, pp. 2338–2347, 2012. 10.1109/TBME.2012.2203820.

[6] P. Massobrio, G. Massobrio, and S. Martinoia, "Interfacing cultured neurons to microtransducers arrays: A review of the neuro-electronic junction models," *Frontiers in Neuroscience*, vol. 10, no. JUN, 2016. 10.3389/fnins.2016.00282.

[7] M. E. J. Obien, K. Deligkaris, T. Bullmann, D. J. Bakkum, and U. Frey, "Revealing neuronal function through microelectrode array recordings," *Frontiers in Neuroscience*, vol. 9, no. JAN, 2015. 10.3389/fnins.2014.00423.

[8] L. Guo, "Perspectives on electrical neural recording: a revisit to the fundamental concepts," *Journal of Neural Engineering*, vol. 17, p. 013001, feb 2020. 10.1088/1741-2552/ab702f.

[9] F. Leva, P. Palestri, , and L. Selmi, "Multiscale simulation analysis of passive and active micro/nano-electrodes for cmos-based in-vitro neural sensing devices," *Philosophical Transactions of the Royal Society A: Mathematical, Physical and Engineering Sciences*, 2021. 10.1098/rsta.2021.0013.

[10] F. Leva, P. Palestri, and L. Selmi, "A simulation study of fet-based nanoelectrodes for active intracellular neural recordings," in *2022 22nd IEEE International Conference on Nanotechnology (IEEE-NANO 2022)*, IEEE, in press.

[11] G. Massobrio, S. Martinoia, and P. Massobrio, "Equivalent circuit of the neuro-electronic junction for signal recordings from planar and engulfed micro-nano-electrodes," *IEEE Transactions on Biomedical Circuits and Systems*, vol. 12, no. 1, pp. 3–12, 2018. 10.1109/TBCAS.2017.2749451.

[12] A. L. Hodgkin and A. F. Huxley, "A quantitative description of membrane current and its application to conduction and excitation in nerve," *The Journal of Physiology*, vol. 117, no. 4, pp. 500–544, 1952. 10.1113/jphysiol.1952.sp004764.

[13] A. J. Bard and L. R. Faulkner, *Electrochemical methods: fundamentals and applications*. John Wiley & Sons, Inc., 2nd ed. ed., 2001.

[14] C. Koch and I. Segev, *Methods in Neuronal Modeling: from Ions to Networks*. MIT Press, 2nd ed. ed., 1998.

[15] R. Jolivet, J. S. Coggan, I. Allaman, and P. J. Magistretti, "Multi-timescale Modeling of Activity-Dependent Metabolic Coupling in the Neuron-Glia-Vasculature Ensemble," *PLoS Computational Biology*, vol. 11, no. 2, 2015. 10.1371/journal.pcbi.1004036.

[16] D. Biolek, V. Biolkova, and Z. Kolka, "Spice models of memristive devices forming a model of hodgkin-huxley axon," in *2013 18th International Conference on Digital Signal Processing (DSP)*, pp. 1–5, IEEE, 2013. 10.1109/ICDSP.2013.6622743.